Lobera González, MP.; Escolástico Rozalén, S.; García Fayos, J.; Serra Alfaro, JM. (2012). Ethylene Production by ODHE in Catalytic Modified Ba0.5Sr0.5Co0.8Fe0.2O3 Membrane Reactors. ChemSusChem. 5:1587-1596. doi:10.1002/cssc.201100747

Lobera González, MP.; Escolástico Rozalén, S.; García Fayos, J.; Serra Alfaro, JM. (2012). Ethylene Production by ODHE in Catalytic Modified Ba0.5Sr0.5Co0.8Fe0.2O3 Membrane Reactors. ChemSusChem. 5:1587-1596. doi:10.1002/cssc.201100747

Ethylene Production by ODHE in Catalytic Modified $Ba_{0.5}Sr_{0.5}Co_{0.8}Fe_{0.2}O_{3-\delta}$ Membrane Reactors

M. Pilar Lobera, Sonia Escolástico, Julio Garcia-Fayos, José M. Serra*

Instituto de Tecnología Química (UPV-CSIC). Universidad Politécnica de Valencia. Consejo Superior de Investigaciones Científicas. Avenida de los Naranjos s/n.46022 Valencia, Spain

Published in CHEMSUSCHEM

doi: 10.1002/cssc.201100747

Abstract

Process intensification by the integration of membranes and high temperature reactors offers several advantages with regard to conventional process schemes, i.e. energy saving, safe operation, reduced plant/unit size and higher process performance, e.g. higher productivity, catalytic activity, selectivity or stability. The present works presents the study of oxidative dehydrogenation of ethane at 850ºC on a catalytic membrane reactor based on a mixed ionic-electronic conducting membrane. The surface of the membrane made of $Ba_{0.5}Sr_{0.5}Co_{0.8}Fe_{0.2}O_{3-\delta}$ has been activated using different porous catalytic layers based on perovskites, the layer was deposited by screen printing and the porosity and thickness has been studied for a catalyst composition. The different catalyst formulations are based on partial substitution of *A*- and *B-site* atoms of doped strontium ferrite-cobaltites ($A_{0.6}Sr_{0.4}Co_{0.5}Fe_{0.5}O_{3-\delta}$ and $Ba_{0.6}Sr_{0.4}BO_{3-\delta}$) and were synthesized by EDTA-citrate complexation route. The use of disk-shaped membrane in the reactor enabled to avoid the direct contact of gaseous oxygen and hydrocarbons and thus to increase the ethylene. High ethylene yields (up to ~ 81 %) were obtained using a catalytic coating based on $Ba_{0.5}Sr_{0.5}Co_{0.8}Fe_{0.2}O_{3-\delta}$ including macropores produced by the addition of graphite platelets in the screen printing ink. The promising catalytic results obtained with this catalytically-modified membrane reactor are attributed to the combination of (1) the high activity as a result of the high temperature and the oxygen species diffusing through the membrane; (2) the control of the oxygen dosing and the low concentration of molecular in the gas phase; and (3) the proper fluid dynamics which enables the appropriate feed contact with the membrane and the rapid removal of products.

Keywords: Ethylene; catalyst, membrane reactor; BSCF; perovskite; ODHE

**corresponding author:* Dr. J.M. Serra, e-mail: jmserra@itq.upv.es, Fax:+34963877809

1. Introduction

Light olefins, especially ethylene and propylene, are the most important basic petrochemicals, which are used to produce other valuable base chemicals, e.g. polyethylene and copolymers, ethylene oxide, acetaldehyde and higher linear olefins and alcohols. Light olefins, like ethylene, are produced mainly by thermal or catalytic cracking. State of the art is an ethane conversion of 69 % at 78 % of ethylene selectivity, implying a ethylene yield of 54 % per pass [1]. These conventional methods present some disadvantages, i.e. (*i*) the product mixture is rather complex and much effort is required for downstream processing; (*ii*) thermal cracking is highly endothermic causing elevated energy costs; (*iii*) under reaction conditions, coke is formed, so frequent discontinuations for reactor cleanup became necessary [2]. One possible alternative to overcome these drawbacks is the oxidative dehydrogenation of ethane (*ODHE*). The advances in selective oxidation of hydrocarbons have been one of the most studied topics in recent decades [1, 3-7]. Two parallel approaches have been followed: (*1*) obtaining a highly active and selective catalyst, and (*2)*, the development of convenient reactor technologies for an effective and safe reactor operation.

An attractive intensification process for the selective oxidation of hydrocarbons integrates a catalytic reactor and a gas separation membrane, e.g. an oxygen permeable mixed ion-electron conducting (*MIEC*) dense membrane [1, 5-17]. This kind of catalytic membranes reactors show several benefits regarding the sustainable production of commodity chemicals, i.e. reducing unit/process volume, safe operation (explosion limits), higher productivity and catalytic performance and energy saving due to the integrated oxygen separation, higher conversion per past and minimization of downstream fractioning and recycle.

Nowadays, the most promising MIEC materials are perovskites with the formula $ABO_{3-\delta}$ (Figure 1). Iron and cobalt-based perovskites usually possess a high electronic conductivity, which is necessary for charge compensation, as well as good ionic conductivity [18]. High oxygen permeation fluxes have been reported even in oxidizing conditions, for single phase materials such as $SrCo_{0.8}Fe_{0.2}O_{3-\delta}$ (SCF) [19], $Ba_{0.5}Sr_{0.5}Co_{0.8}Fe_{0.2}O_{3-\delta}$ (BSCF) [20, 21], $La_{0.6}Sr_{0.4}Co_{0.2}Fe_{0.8}O_{3-\delta}$ (LSCF) [22]. The materials showing the highest oxygen permeability are based on $Ba_{0.5}Sr_{0.5}Co_{0.8}Fe_{0.2}O_{3-\delta}$ (BSCF) which was first reported by Shao et al. [23]. The mechanism of a dense MIEC membrane for selective oxidation of hydrocarbons includes the following steps: the molecular oxygen in air is reduced on surface of the membrane in the feed side to form oxygen-ions (O^{2-}), and then O^{2-} are transported selectively through the membrane under the driving force of a gradient in oxygen chemical potential. The flux of O^{2-} is charge compensated by a simultaneous flux of electrons or electron holes. And finally the lattice oxygen (O^{2-}) will react quickly with the ethane on the membrane surface (reaction side) before it recombines to molecular oxygen.

This approach combines the ODHE reaction and oxygen separation into a catalytic MIEC membrane reactor. Although MIEC membranes are also catalytically active [7, 12, 14, 16] in ODHE reaction, it would be possible to increase its ethylene yield by using a proper catalyst on the membrane surface. In general, two strategies have been used for this purpose: (1) a catalyst packed-bed is attached to the membrane surface; and (2) the membrane surface is modified by coating a catalytic layer using different methods, e.g. deposition of a very thin layer of catalyst by spin casting or wash-coating technique.

The addition of catalytic material on the membrane surface may allow the rate of surface reactions to be increased. However, catalysts must be stable at higher temperatures. The use of catalyst based on perovskite compounds is an interesting approach since ODHE reaction might take place using directly surface oxygen species diffusing from the perovskite bulk. Partial substitution of *A* or *B* site cations in the perovskite lattice by other metal cations with different ionic radii, oxidation states and redox behavior may allow the promotion of the catalytic activity in ODHE reaction and ionic transport of oxygen, typically due to the formation of a higher number of oxygen vacancies in the perovskite crystal and variation of O-cation bond strength [18].

In this study, different catalysts modifying the BSCF membrane were used to study their catalytic performance in the ODHE reaction at 850ºC and different ethane concentrations in the feed were considered. These catalysts consist of iron-based perovskites while the effect of the catalytic behaviour was studied when different cations were incorporated in the A and B crystallographic sites. The catalysts were applied as ~15µm-thick porous coatings onto disk-shaped monolithic membranes made of BSCF. Moreover, the effect of the catalyst layer thickness and macroporosity on the catalytic membrane performances was investigated.

2. Experimental

Dense membrane disks made of $Ba_{0.5}Sr_{0.5}Co_{0.8}Fe_{0.2}O_{3-\delta}$ (*BSCF*) were prepared by solid state reaction. The BSCF powder was provided from IKTS Fraunhofer (Germany) and it was preconditioned by ball milling in acetone suspension in order to decrease the grain size obtained prior pelletizing. The disk-shape planar membranes with diameter of 15 mm and 0.8 mm thickness were prepared by uniaxial pressing at 150 kN and ulterior densification of the disk was achieved by sintering in air for 5 h at 1100 ºC (2 ºC min^{-1} ramp).

Different catalyst formulations based on MIEC perovskites with the formula $ABO_{3-\delta}$ were considered. The *A*- and *B-site* doped strontium ferrite-cobaltite compounds ($A_{0.6}Sr_{0.4}Co_{0.5}Fe_{0.5}O_{3-\delta}$ and $Ba_{0.6}Sr_{0.4}BO_{3-\delta}$) were synthesized by EDTA-citrate complexation route [24, 25]. Stoichiometric amounts of metal precursor nitrates were weighed and solved together in the minimum amount of water. Citric acid was used as chelating agent, in a ratio (citric acid):(metal ions) of 2:1. Metal complexation was

promoted by heat treatment, i.e., the solution was heated to 100 ºC to form a viscous gel and then was maintained at 200 ºC for 6 h. The resulting foam product was then calcined in air to remove carbonaceous matter and favour the mixed oxide crystallization. The maximum calcination temperature to get this was around 1050 ºC.

The obtained catalysts were characterized by X-ray diffraction (XRD) on a Philips X'Pert Pro equipped with an X'celerator detector using monochromatic Cu Kα radiation. XRD patterns were recorded in the 2θ range from 20 to 90 º and analysed using X'Pert Highscore Plus software (PANalytical).

Temperature programmed desorption of oxygen (O_2-TPD) measurements were performed in order to observe the oxygen release with temperature. The powdery catalyst (20 mg) was ground and sieved to a particle size of 200 – 400 μm. Each sample was placed in a quartz reactor and it was heated up in air until 1000 ºC and cooled in the same atmosphere. Then the sample was heated up at 10 ºC/min up to 1000 ºC in He atmosphere and the oxygen release was monitored by following the characteristic mass (m/e) = 32 (O_2) with a mass spectrometer Omnistar (Balzers).

The screen-printing method was used to modify the membrane surface. The screen-printing inks were prepared by mixing the ball-milled powders with a solution of 94 wt.% terpineol and 6 wt.% ethylene cellulose. The ink homogenization was conducted using a three-roll mill; this step was repeated three times. The coating membranes were calcinated in air for 2 h. The calcination temperature results from the diverse sintering activities of each catalytic material, thereby the BSCF coating was sintered at 1010 ºC and the other MIEC coatings, at 1050 ºC. The microstructure of the catalytic modified membrane reactors was analyzed by SEM and EDS in a JEOL JSM6300 electron microscope.

Oxygen permeation studies and ODHE experiments were carried out in the same experimental set-up [12]. The catalytic modified BSCF membrane reactor is illustrated schematically in Figure 2. The disk-shape planar membrane was sealed using gold gaskets. Synthetic air was fed to the feed side while argon or diluted ethane was used as sweep gas on the reaction side (permeate). Gas chromatography (micro-GC Varian CP-4900 equipped with Molsieve5A, Pora-Plot-Q glass capillary and CP-Sil modules) allowed complete analysis of gases at both sides of the membrane. Flow and composition of the gas streams were individually controlled. Membrane gas leak-free conditions were confirmed by continuously monitoring the nitrogen concentration in the product gas stream. An acceptable sealing was achieved when the ratio between the oxygen flow leak and the oxygen flux was lower than 1%. The temperature was measured by a thermocouple attached to the membrane (reaction side). A PID controller maintained temperature variations within 2 ºC of the set point.

Data reported are achieved at steady state after half an hour in as stabilization time and GC analysis has been repeated three times to minimize analysis error. Indeed, the obtained experimental error is below 0.5 %. The deviation in reproducibility with regard

to oxygen permeation flux for the test of identical membrane reactors is below ± 2.5 %. Carbon balances were always better than ±2.5% and significant coke formation was only initially observed during the reaction startup. Ethane conversion, ethylene selectivity and ethylene yield were defined as follows:

$$X_{C_2H_6} = \frac{\sum_i \frac{n_i}{2} F_i^{out} - F_{C_2H_6}^{out}}{\sum_i \frac{n_i}{2} F_i^{out}} x100 \quad \text{(Eq.1)}$$

$$S_i = \frac{\frac{n_i}{2} F_i^{out}}{\sum_i \frac{n_i}{2} F_i^{out} - F_{C_2H_6}^{out}} x100 \quad \text{(Eq.2)}$$

$$\boldsymbol{Y}_{\boldsymbol{C_2H_4}} = \frac{\boldsymbol{X}_{\boldsymbol{C_2H_6}} \boldsymbol{S}_{\boldsymbol{C_2H_4}}}{100} \quad \text{(Eq.3)}$$

where *i* includes all the components with carbon atoms in the permeate gas stream, n_i is the number of carbon atoms of component *i*, and F_i is its molar flow.

3. Results and Discussion

3.1. Structural characterization and temperature programmed experiments

Figure 3 shows the XRD patterns for the different perovskite materials: $Ba_{0.5}Sr_{0.5}Co_{0.8}Fe_{0.2}O_{3-\delta}$ (*BSCF*), $Nd_{0.6}Sr_{0.4}Co_{0.5}Fe_{0.5}O_{3-\delta}$ (*NdSCF*), $La_{0.5}Ce_{0.1}Sr_{0.4}Co_{0.5}Fe_{0.5}O_{3-\delta}$ (*LaCeSCF*) and $Ba_{0.6}Sr_{0.4}FeO_{3-\delta}$ (*BSF*) were well indexed as a cubic perovskite structure. Moreover, LaCeSCF compound presents peaks corresponding to the cubic geometry for CeO_2 while $Sm_{0.6}Sr_{0.4}$ $Co_{0.5}Fe_{0.5}O_{3-\delta}$ (*SmSCF*) presents peaks corresponding to the orthorhombic symmetry domains [26, 27].

Figure 4 showed the qualitative O_2-TPD profiles of the catalysts. With the increase of temperature under helium (2·ppb O_2), principally B-site cations in the perovskite lattice were progressively thermally reduced to a lower oxidation state. At the same time, some molecular oxygen was formed to maintain the charge neutrality. During the thermal reduction of cobalt and iron cations, oxygen ions in the perovskite bulk move toward the surface, where they combine to form molecular oxygen and release from the surface into the surrounding atmosphere. In general, desorption peaks plotted from the perovskite-like mixed oxides after O_2-TPD analysis contain two kinds of oxygen species from so-called α- and β-oxygen, respectively. In the present case, the low temperature peak (α-oxygen) can be attributed to oxygen release related to the reduction of highly-valent cations, e.g. Fe^{+4} and Co^{+4}, which are stable in the perovskite lattice at low temperatures and high oxygen partial pressures[28]. At room temperature both

metals ar present as a mixture of +3 and +4 cations. The desorption peak appeared at high temperatures (β-oxygen) is ascribed to the to the reduction[29] of trivalent cations to form principally divalent cations, e.g. $Co^{+3} \rightarrow Co^{+2}$. One should note (Figure 4) that in the BSF sample (containing no cobalt), only there appeared a peak at 420 ºC, which might be ascribed to the depletion of the most reducible cations (Fe^{+4}). From these measurements, the proportion between Fe^{+4} and Fe^{+3} cannot be determined. BSF sample is significantly less reducible than the Co-containing counterpart (BSFC), as expected from the higher strength of the Fe-O bond and higher stability of Fe^{+4} cation. While for the rest of catalysts two reduction peaks were observed at high and moderate temperature. The first oxygen desorption started at ~400 ºC and ~450 ºC for the BSCF and SmSCF samples respectively. And in the case of NdSCF and LaCeSCF samples, the onset temperature for oxygen desorption was at temperatures above 500 ºC. Moreover, the oxygen release at low temperature indicates that the Co-O and/or Fe-O bond energy is weakened because of the enlarged cell volume [30]. The second oxygen desorption peak was observed at T > 800 ºC, for BSCF, SmSCF, NdSCF and LaCeSCF samples, which could be ascribed to both (i) the mobile lattice oxygen and (2) the higher redox (catalytic) activity in the temperature range used for ODHE reaction in the present work.

3.2. Oxygen permeability. Influence of the catalyst coating

The oxygen permeation flux through the MIEC membrane is a key factor in the behavior of the catalytic membrane reactor for selective oxidations of hydrocarbons [7]. Figure 5 presents oxygen permeation data in an Arrhenius arrangement obtained using Ar and Ar/CH_4 (85/15 vol.) as sweep gas for *(i)* the reference membrane reactor (bare membrane reactor with polished surface), and (*ii*) the catalytic modified membrane reactor[1]. The oxygen permeation flux through the membrane, $J(O_2)$ (ml min^{-1} cm^{-2}), was calculated considering the oxygen content measured in reaction side of the permeation assembly, the sweep gas flow rate and the area of the membrane surface exposed to the flowing gas. The oxygen permeation flux was determined in the temperature range of 650-1000 ºC.

As shown in Figure 5, $J(O_2)$ presents a classic behavior of perovskite-type membranes. In a thick MIEC membrane, the oxygen permeation process can be limited by the bulk oxygen-ions diffusion, the oxygen surface exchange kinetics (this process becomes more relevant for highly permeable materials such as BSCF and/or for small membrane thickness), or a combination of them [9, 18]. $J(O_2)$ increased with the temperature as expected. Furthermore, two different temperature domains become evident as a change in the slope of the curve with an increasing temperature was shown. Thus, the apparent activation energies (E_a) for the oxygen transport process through the membrane changes

[1] The catalytic coating is a porous BSCF layer (~13μm thickness)

according to the temperature range investigated (Table 1). Similar results were obtained with these two membrane reactors at higher temperatures where the bulk diffusion of oxygen ions is the limiting step and $J(O_2)$ should be given by Wagner equation[2] [18]. Furthermore, comparable values of activation energy for thick BSCF bare membrane were previously reported [15, 31].

The oxygen permeation flux is increased 2.5-fold when diluted methane (Ar/CH_4; 85/15 vol.) is used as sweep gas. The upturn in the $J(O_2)$ was expected due to the increase in the separation driving force, i.e., log pO_2 (air)/pO_2 (sweep) from 0.88 to 3.85 (bare membrane) and 1.16 to 4.02 (membrane with a catalytic coating) when diluted methane is used as sweep gas[3]. Moreover, the use of hydrocarbons as sweep gas may lead to the modification of surface processes related to *(i)* a severe change in the surface vacancy concentration and *(ii)* the reduction of redox species, i.e. Fe and Co cations, involved in the oxygen activation.

The catalytic modification of the membrane leads to the increase in the $J(O_2)$ reached in the lower temperature range with respect to the bare membrane. This improvement is more significant since the oxygen surface exchange reaction is controlling the permeation process and surface catalytic promotion enables increasing the reaction rates. Moreover, the catalytic surface modification of the membrane leads to lower activation energy for the oxygen permeation process which is ascribed. When a thick membrane is used, this effect is especially evident in the low temperature range.

3.3. Catalytic performance in the ODHE reaction

Figure 6 shows the catalytic behaviour (*ethylene yield, Y_{C2H4}*) in the ODHE reaction for different membrane reactors (*MR*) at 850 ºC. When the ODHE reaction is carried out at high temperatures, the results are not only produced through catalytic conversion and a certain contribution of gas-phase reaction takes place, usually involving additional oligomerization and coking reactions. The use of an inert gastight membrane made of Al_2O_3 (no oxygen permeable material) enabled determining the contribution of the gas-phase reaction to the global process. The existence of active oxygen species (i.e. associated to lattice oxygen - inert MR) on the MIEC membrane surface is expected to

---

[2] $$\boldsymbol{J(O_2)} = \frac{\boldsymbol{RT}}{16\boldsymbol{LF}^2}\int_{\boldsymbol{pO_2''}}^{\boldsymbol{pO_2'}} \sigma_{\boldsymbol{amb}}(\boldsymbol{pO_2})\,\boldsymbol{d}\ln \boldsymbol{pO_2}$$

where *$J(O_2)$* is the oxygen permeation rate, *R* gas constant, *F* Faraday constant, *L* membrane thickness, *pO_2'* and *pO_2"* the oxygen partial pressure at the high pressure side and the low pressure side, respectively. σ_{amb} (S m^{-1}) is the average ambipolar conductivity.

[3] Here, it is considered the ideal case in which it is assumed that the permeate pO_2 corresponds to the sweep gas (diluted methane). For the Wagner equation integration, it is also assumed that ionic conductivity does not depends significantly on pO_2 and this is negligible with respect to the electronic conductivity.

allow the ODHE reaction to occur via ethyl radical formation on the surface of the membrane, and the later formation of ethylene in the gas-phase. The experimental results of figure 6 confirmed the better performance achieved by the MIEC membrane reactors, especially when a catalytic porous coating made of BSCF is applied. When no gaseous O_2 was co-fed using the inert MR configuration, the ethylene yield obtained is lower than the Y_{C2H4} achieved when a MIEC-MR was used. Moreover, when ethane was co-fed with oxygen using the inert MR configuration, the Y_{C2H4} diminished substantially due to the deep oxidation of reaction products with molecular oxygen. It can be inferred from this catalytic behaviour that the reactivity of lattice oxygen (O^{2-}) is much lower, i.e. selective, than that of gaseous oxygen, since O_2 co-feeding leads to the deep oxidation of ethane and ethylene, and the selectivity of ethylene is reduced [7, 12]. Moreover, it can be ascertained that, despite the fact that an important contribution of gas-phase reaction exists, as inferred from the significant H_2 concentration in the product mixture (Table 2), the coupled effects of oxygen permeation, catalytic oxidation and fluid dynamics [32] at the membrane surface and reactor chamber play a key role in the ethane conversion process. Furthermore, when catalyst modified membrane reactors are employed, an important enhancement in Y_{C2H4} is observed.

With regard to product selectivity, the integration of the MIEC membrane allows reducing the selectivity toward heavier compounds as C_4, benzene and specially coke, due to the minimization of radical-driven oligomerization reactions and in a lesser extent to deep hydrocarbon oxidation and aromatization. For the case of the anaerobic experiment in the inert MR, the oligomerization and coking issues were very pronounced while oxygen co-feeding resulted in the deep oxidation of the produced olefins (see Figure S1 in supporting material).

3.4. Effect of the composition of the catalytic layer

In order to study the role of the *A/B-site* cation nature in the perovskite structure, different compositions of the catalytic layer were experimentally tested on the catalytic MIEC-MR. The catalytic activity of *LnSCF* oxides (*Ln*=Ba, La, Ce, Nd, Sm) depends on both *(1)* the lanthanide element incorporated in the *A-site* and *(2)* the transition metal added in the *B-site* in the perovskite structure. Figure 7 shows the SEM morphologies of catalytic modified BSCF membranes after ODHE reaction test. Although some pores appear on the cross-section of the membrane, they are proved to be closed-pores by helium leakage test. The thickness of the catalytic layers was determined to be ~ 13 μm from SEM images. The catalytic layers have an open microstructure with macropores and a homogeneous thickness. A lower particle size was observed, although they present little apparent porosity. Finally, the integrity of all catalytic porous layers was conserved during the whole reaction tests, as deduced by SEM analysis. The catalytic membrane reactor stability was assessed for several days although it is well-know that BSCF is prone to carbonate in the presence of CO_2 at temperatures below 850ºC [33]. Post-mortem XRD analysis of the catalytic layers indicates the formation of carbonates

(see figure S2 in supporting material). For the short operation time (two weeks), the catalytic behavior was not affected by the formation of these carbonate domains. In order to improve the long-term stability of the membrane reactor under realistic operating conditions, the use of thin protective layers on Ba/Sr-based perovskite membranes [34] or the use of membrane materials with higher stability against carbonation such as doped ceria as supported thin layers [35, 36] becomes necessary.

Figure 8 collects the results obtained in the ODHE test performed using different BSCF-MR functionalized with different catalytic coatings. Diverse tests were carried out by keeping the residence time constant and varying the ethane concentration in the feed reaction mixture. The results obtained in a previous study have shown that the ethane conversion increases with the reaction temperature whereas the selectivity declined slightly and remained always at high values for a given feed composition [12]. A thoroughly study of the effect of operating conditions on BSCF-based membrane reactor for the oxidative dehydrogenation of ethane is reported elsewhere [33]. To compare the catalytic performance of the BSCF-MR, the reaction temperature was fixed at 850 ºC. As previously inferred from Figure 6, the use of a catalytic layer had a significant effect in the results reached, regarding to the bare membrane with polished surface. Namely, it allows increasing the ethylene yield in more than 5 % (Y_{C2H4} ~ 79.8 % at 2.3 % C_2H_4). As expected, ethylene yield decreases when the ethane concentration increases in the feed although the ethylene productivity rises monotonically (see Figure S3 in supporting material). Moreover, the increase in catalytic activity for modified membranes is just accompanied by a slight drop in ethylene selectivity. Ethylene is the main product obtained using the membranes with different catalytic layers while H_2, CO_x, CH_4, C_3 and C_4-hydrocarbons are also observed in minor amounts. Table 2 summarizes the catalytic results obtained for the different catalyst at a fixed ethane % in the feed. In the whole range of operating conditions studied, the oxygen concentration on the products gas stream was less than 50 ppm and this might suggest that the selective oxidation of ethane takes place through a catalytic pathway rather than a gas-phase reaction [7].

Surface and related lattice oxygen of perovskite catalyst should be involved in the different steps of the ODHE reaction scheme. As a consequence, the changes induced by doping in A and B-cations, in both the mixed ionic-electronic conductivity[18] and the redox behavior at high temperature may have an impact in the final activity and selectivity of the ODHE reaction. Furthermore, the presence of cations in the catalyst with higher oxidation states is expected to suppress some of their basicity [37] while the incorporation of A cations with mixed valence, i.e. Sm (II, III) and Ce (III, IV), may alter the catalytic redox behavior. The use of catalyst with lower acidity implies an improvement in the properties of the catalysts for ODHE reaction because they inhibit secondary reactions such as cracking, aromatization and oligomerization. The ethylene selectivity increases as follows: *NdSCF* < *BSF* < *SmSCF* < *BSCF*, according to the present results and for an ethane iso-conversion of 88 % (Figure 8). LaCeSCF coating is not discussed since only conversions below are achieved. Furthermore, high ethylene

selectivity (over 90 %) was achieved when catalytic layers of SmSCF or BSCF were used. The best results are obtained with those materials exhibiting important oxygen desorption peaks in helium (Figure 4). For comparison, the catalytic layer of NdSCF showed the lowest ethylene selectivity and the highest selectivity towards C_4 (S_{C4}) hydrocarbons. The lowest S_{C4} was obtained when LaCeSCF, which presents the highest reducibility at high temperature, was used as catalytic layer; maybe due to relative basicity of lanthanum is higher than the others lanthanides compounds, so La-based catalytic layer present lower tendency to the oligomerization and aromatization of the formed ethylene. Our results show that the use of BSCF as catalytic layer enable reaching the highest ethylene selectivity, while it showed a low S_{COx} and S_{C4} compared to the others catalytic layers (Table 2), so it has obtained the highest ethylene yield. In contrast, NdSCF shows the lowest yield values.

3.5. Effect of the layer porosity and thickness

Given these results, BSCF catalytic layer was selected to analyze the effect of the textural properties and the thickness of the porous catalyst layer. The porosity of the catalytic layer in modified MIEC-MR is a crucial issue principally determining the catalytic activity and in a less extent the selectivity. Such a behavior was attributed to *(i)* an increase of the available catalytic surface area and *(ii)* an enhancement of the gas exchange due to the fast evacuation of ethylene and the minimization of secondary reactions. Consequently, the porous microstructure of the catalytic layer could have an important role in the catalytic performance of MIEC-MR; in particular, when the reaction scheme involves the interaction among gas-phase molecules and the lattice oxygen, as for the ODHE reaction. Figure 9 shows the SEM pictures of fracture cross-section for three catalytic layers of BSCF after ODHE reaction test. The catalytic layer shown in Figure 9b shows higher porosity achieved by the incorporation in the screen-printing ink of graphite (Aldrich) with platelet morphology (diameter of several tens of microns). The addition of graphite (5% wt.) was aimed to promote the formation of macropores for a fast oxygen gas transport. The porosity of the catalytic layers was optimized by using graphite as pore former in the screen-printing ink. Different thicknesses of the catalyst layer were used in these ODHE experiments: 13 μm (Figure 9b) and 26 μm (Figure 9c).

The influence of the layer porosity on the catalytic performance was studied. The ODHE experiments were carried out under equal experimental conditions in different catalytic BSCF-MR. Figure 10 compares the results obtained in the ODHE experiments employing a bare membrane with the polished surface as reference MR and two modified MR with catalytic layers of BSCF with different porosity. As said above, the oxygen species (O^{2-}) are transported through the BSCF membrane from the feed to the reaction side, where they react rapidly with ethane on the catalyst surface before recombination to form molecular oxygen. This membrane process makes it possible to reach higher ethylene selectivity due to the complete control over the contact mode of

hydrocarbons, oxygen and the catalyst active sites. The use of a porous catalytic layer with extra macroporosity has produced an increase in the ethylene yield (up to Y_{C2H4} ~ 81 %). The presence of the macroporosity allowed also improving the oxygen flux through the membrane, as unambiguously proved when using only argon as sweep gas. This improvement may be ascribed to the higher surface area for oxygen exchange and the better gaseous oxygen transport through the porous coating [20, 25]. As a consequence, the rise in Y_{C2H4} could be related to the higher oxygen flux through the membrane, the higher surface area available on the catalytic coating and improved gas transport through the coating.

The thickness of the catalytic layer may affect the oxygen permeation process, increasing the gas diffusion resistance through this porous layer, especially at lower temperatures. $J(O_2)$ ~ 1 ml min^{-1} cm^{-2} was reached at 750 ºC in the MR in a catalytic layer of 13 μm and $J(O_2)$ ~ 0.8 ml min^{-1} cm^{-2} was obtained with a catalytic layer of 26 μm. Likewise, the thickness of the catalytic layer, i.e. the amount of catalyst used in the reaction, would affect the catalytic ODHE performance. A thicker catalyst layer (Figure 11b) had a positive effect on the catalytic activity of the membrane reactor, as the ethane conversion increases with spatial time (Figure 11a). However, a shorter residence time involves a lower probability of secondary reaction such as oxidation or oligomerization of the ethylene produced, so selectivity increases. The combination of these effects caused a slight decrease in Y_{C2H4} when reducing the thickness of the catalytic layer while leaving the reaction conditions intact (Figure 11b). From the inset of Figure 11b, it can be inferred that the variation in the layer thickness results in a mere increase in the catalytic activity (conversion) but does not alter the isoconversion selectivity.

Figure 12 summarizes the catalytic results from previous works published on ODHE reaction using perovskite-type ceramic MR and all results obtained in this work. Mirodatos and co-workers [14] reported an ethylene yield of 75 %, with a MR using disk shaped MIEC ($Ba_{0.5}Sr_{0.5}Co_{0.8}Fe_{0.2}O_{3-\delta}$) membrane modified with Pd nano-clusters and 73 % of Y_{C2H4} when the membrane surface was activated using a thin layer of V/MgO; in both cases at 777 ºC and using 25 % v/v of C_2H_6 in the feed stream. Akin and Lin [8] reported an ethylene yield of 56 % (per pass) with a dense tubular ceramic membrane reactor made of $Bi_{1.5}Y_{0.3}SmO_3$ (fluorite structure) at 875 ºC and 10 % of C_2H_6 in the feed stream. Yang et al. [7] reported an ethylene selectivity of 80 % at 84 % ethane conversion by using a dense MIEC ($Ba_{0.5}Sr_{0.5}Co_{0.8}Fe_{0.2}O_{3-\delta}$) as membrane in a co-feed reactor. Caro et al. [38] investigated the ODHE using a dense perovskite hollow-fiber membrane of $BaCo_xFe_yZr_ZO_{3-\delta}$ by using a standard commercial dehydrogenation catalyst (Actisorb 410, Südchemie, Cr_2O_3 on Ca aluminate), they obtained an ethylene yield of 43% and ethylene selectivity of 67 % at 725 ºC and 30 % v/v of C_2H_6 in the feed stream. Wang et al. [16] reported an ethylene selectivity of 67.4 % at 80 % ethane conversion by using a dense MIEC ($Ba_{0.5}Sr_{0.5}Co_{0.8}Fe_{0.2}O_{3-\delta}$) as membrane at 850 ºC and 10 % v/v of C_2H_6 in the feed stream.

In these works, there exists a wide dispersion regarding the temperature of reaction, catalysts and reactor configuration. The higher ethylene yield obtained in this study with catalytically-modified membrane reactors can be ascribed to the combination of following aspects: *(1)* high activity as a result of the high temperature and the oxygen species diffusing through the membrane; *(2)* control of the oxygen dosing and the low concentration of molecular oxygen in the gas phase; (3) the improved catalytic activity of the porous layers, due to the enlarged surface area (regarding the bare membrane), which influences both the hydrocarbon reaction kinetics and the oxygen permeation, and *(4)* proper fluid dynamics which enables the appropriate feed contact with the membrane and the rapid removal of products.

Finally, catalytic tests at 850ºC using much higher ethane concentrations in the feed stream were conducted on a membrane coated with a BSCF layer with macroporosity . Figure 13 shows the ethylene productivity as a function of the ethane concentration as well as the corresponding ethylene selectivity and ethane conversion values (Inset). Very high ethylene productivities can be achieved when high ethane concentrations and high gas flow rates (Q_{feed} = 400 mL·min) are employed. This high productivity is possible due to (1) the high ethylene selectivity reached at high conversions and (2) the relatively high conversion degrees attained at high ethane concentration in the feed. Moreover, the contribution of gas-phase dehydrogenation reaction at 850 ºC and the proper fluid dynamics in the reaction chamber, which enables the rapid evacuation of reaction products, are also very beneficial in this case. The stability of the catalytic membrane reactor operation was assessed for several days and no major degradation was observed. This short-term stability is ascribed to (1) the low coke formation rate combined with the concomitant oxygen permeation and (2) the negligible membrane carbonation caused by the low stability of alkali-earths carbonates above 800 ºC and low CO_2 concentration, although BSCF materials is not stable under this operating conditions for long periods [39].

4. Conclusions

Oxidative dehydrogenation of ethane has been studied at 850ºC on a catalytic membrane reactor based on a mixed ionic-electronic conducting membranes made of $Ba_{0.5}Sr_{0.5}Co_{0.8}Fe_{0.2}O_{3-\delta}$. The catalytic layer was deposited by screen-printing method. Different catalysts formulations are considered varying the *A/B-site* cation in the perovskite structure. Moreover, the porosity and thickness of the catalytic layer has been studied for a given catalyst formulation. The use of a disk-shaped membrane in the reactor allows avoiding the direct contact of molecular oxygen and hydrocarbons and consequently high ethylene selectivity is achieved. High ethylene yields (up to ~ 81 %) were obtained using a membrane catalytic coating based on $Ba_{0.5}Sr_{0.5}Co_{0.8}Fe_{0.2}O_{3-\delta}$ including macropores produced by the inclusion of graphite platelets in the screen printing ink. Moreover, high productivity values were reached when high ethane concentrations (up to 85% in Ar) in the feed stream were employed. The interesting

catalytic results obtained with this membrane reactor are ascribed to the combination of (*1*) the high activity due to the high temperature and the active oxygen species diffusing through the membrane; (*2*) the control of the oxygen dosing and the low concentration of molecular in the gas phase; and (*3*) adequate fluid dynamics which enables the proper feed contact with the membrane and the rapid removal of the formed ethylene.

The use of the MIEC membranes with catalytic coatings provides a promising route for ethylene production. The use of catalytic coatings in the MIEC membranes allowed improving the results obtained with uncoated membranes. The improvement in long-term stability of the reactor membrane under realistic operating conditions will involve the use of thin protective layers on Ba/Sr-based perovskite membranes [34] or the use of intrinsically stable materials such as doped ceria as supported thin layers [35, 36]. This kind of membrane reactor systems may find application in other oxidative dehydrogenation reactions albeit the operating conditions should be precisely selected due to the higher activities of the corresponding reaction products.

Acknowledgements

Financial support by the Spanish Ministry for Science and Innovation (Project ENE2008-06302, ENE2011-24761 and FPI Grant JAE-Pre 08-0058), EU through FP7 NASA-OTM Project (NMP3-SL-2009-228701), and the Helmholtz Association of German Research Centres through the Helmholtz Alliance MEM-BRAIN (Initiative and Networking Fund) is kindly acknowledged. Authors thank S. Jimenez for material preparation, M. Fabuel for TPD experiments, and FZJ for SEM analysis of BSCF catalytic layer.

Figure Captions

Figure 1. The structure of perovskite $ABO_{3-\delta}$ with the presence of oxygen vacancies.

Figure 2. Schematic of the quartz membrane reactor design.

Figure 3. XRD patterns. $A_{1-x}Sr_xCo_{0.5}Fe_{0.5}O_{3-\delta}$ and $Ba_{0.6}Sr_{0.4}B_yO_{3-\delta}$ perovskite powders. (▪) Marked peaks correspond to the cubic symmetry of CeO_2. (▲) marked peaks correspond to the orthorhombic symmetry coming from Sm-based compositions [26, 27].

Figure 4. O_2-TPD profiles obtained from $A_{1-x}Sr_xCo_{0.5}Fe_{0.5}O_{3-\delta}$ and $Ba_{0.6}Sr_{0.4}B_yO_{3-\delta}$ perovskite powders: (a) $Ba_{0.6}Sr_{0.4}FeO_{3-\delta}$ (BSF); (b) $Ba_{0.5}Sr_{0.5}Co_{0.8}Fe_{0.2}O_{3-\delta}$ (BSCF); (c) $Sm_{0.6}Sr_{0.4}Co_{0.5}Fe_{0.5}O_{3-\delta}$ (SmSCF); (d) $Nd_{0.6}Sr_{0.4}Co_{0.5}Fe_{0.5}O_{3-\delta}$ (NdSCF); and (e) $La_{0.5}Ce_{0.1}Sr_{0.4}Co_{0.5}Fe_{0.5}O_{3-\delta}$ (LaCeSCF).

Figure 5. Temperature dependence of oxygen permeation flux through different catalytic membranes reactors. $Q_{Sweep\text{-}gas}$ = 65 ml min^{-1}, Q_{Air} = 60 ml min^{-1} (synthetic air; pO_2=0.21 atm). (a) Ar as sweep gas; (b) Ar/CH_4 (85/15vol.) as sweep gas.

Figure 6. Ethylene yield obtained in inert membrane reactor of dense Al_2O_3 and BSCF membrane reactors. Catalytic layer made of BSCF. T = 850 ºC, $Q_{Reaction\ side}$= 400 ml min^{-1}, ethane diluted with argon; $Q_{Feed\ side}$= 210 ml min^{-1} (pO_2=0.04 atm).

Figure 7. SEM images of the fracture cross-section of the different catalytic layers on BSFC membranes after catalytic test. (a) Bare membrane (polished surface); catalytic layer: (b) $Ba_{0.5}Sr_{0.5}Co_{0.8}Fe_{0.2}O_{3-\delta}$ (BSCF); (c) $Sm_{0.6}Sr_{0.4}Co_{0.5}Fe_{0.5}O_{3-\delta}$ (SmSCF); (d) $Nd_{0.6}Sr_{0.4}Co_{0.5}Fe_{0.5}O_{3-\delta}$ (NdSCF); (e) $La_{0.5}Ce_{0.1}Sr_{0.4}Co_{0.5}Fe_{0.5}O_{3-\delta}$ (LaCeSCF); (f) $Ba_{0.6}Sr_{0.4}FeO_{3-\delta}$ (BSF).

Figure 8. Comparative results on ethylene selectivities at different degrees of ethane conversions derived from the experiments performed with the catalytic modified BSCF-MR used in this study. T = 850 ºC, $Q_{Reaction\ side}$= 400 ml min^{-1}, ethane diluted with argon; $Q_{Feed\ side}$ = 210 ml min^{-1} (pO_2=0.04 atm).

Figure 9. SEM images of the fracture cross-section of the $Ba_{0.5}Sr_{0.5}Co_{0.8}Fe_{0.2}O_{3-\delta}$ (BSCF) catalytic layer on BSFC membranes after catalytic test. (a) 12 μm thickness, (b) pore former in the screen-printing ink is added, 13 μm thickness, (c) pore former in the screen-printing ink is added, 26 μm thickness.

Figure 10. Ethylene selectivity vs ethane conversion for experiments performed with BSCF membrane reactors. Different porosity of the catalytic layer is considered. T = 850 ºC, $Q_{Reaction\ side}$= 400 ml min^{-1}, ethane diluted with argon; $Q_{Feed\ side}$ = 210 ml min^{-1} (pO_2=0.04 atm).

Figure 11. Catalytic performance of the modified BSCF membrane reactors in the ODHE reaction as a function of the thickness of the catalytic layer: 13 μm and 26 μm; (a) Ethane conversion and ethylene selectivity; (b) Ethylene yields obtained in BSCF membrane reactors. T = 850 ºC, $Q_{Reaction\ side}$= 400 ml min^{-1}, ethane diluted with argon; $Q_{Feed\ side}$ = 210 ml min^{-1} (pO_2=0.04 atm).

Figure 12. Catalytic performance of the modified BSCF-MR in the ODHE reaction in terms of ethylene selectivity as a function of ethane conversion. Data for various catalytic dense membrane reactors reported in literature: (1) Mirodatos et al. [14]; (2) Akin and Lin [8]; (3) Yang et al. [7] ; (4) Caro et al. [38]; (5) Wang et al. [16].

Figure 13. Catalytic tests using high ethane concentrations in the feed stream. Ethylene productivity obtained using the catalytic coating and (Inset) ethylene selectivity versus ethane conversion. T = 850 ºC, $Q_{Reaction\ side}$= 400 ml min^{-1}, ethane diluted with argon.

Figure 1

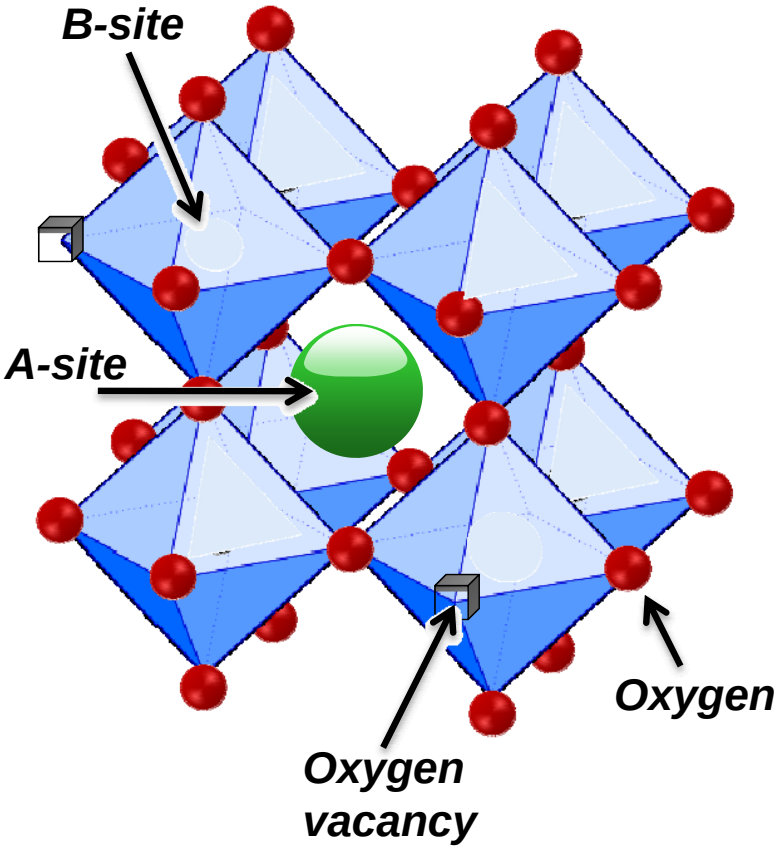

Figure 2

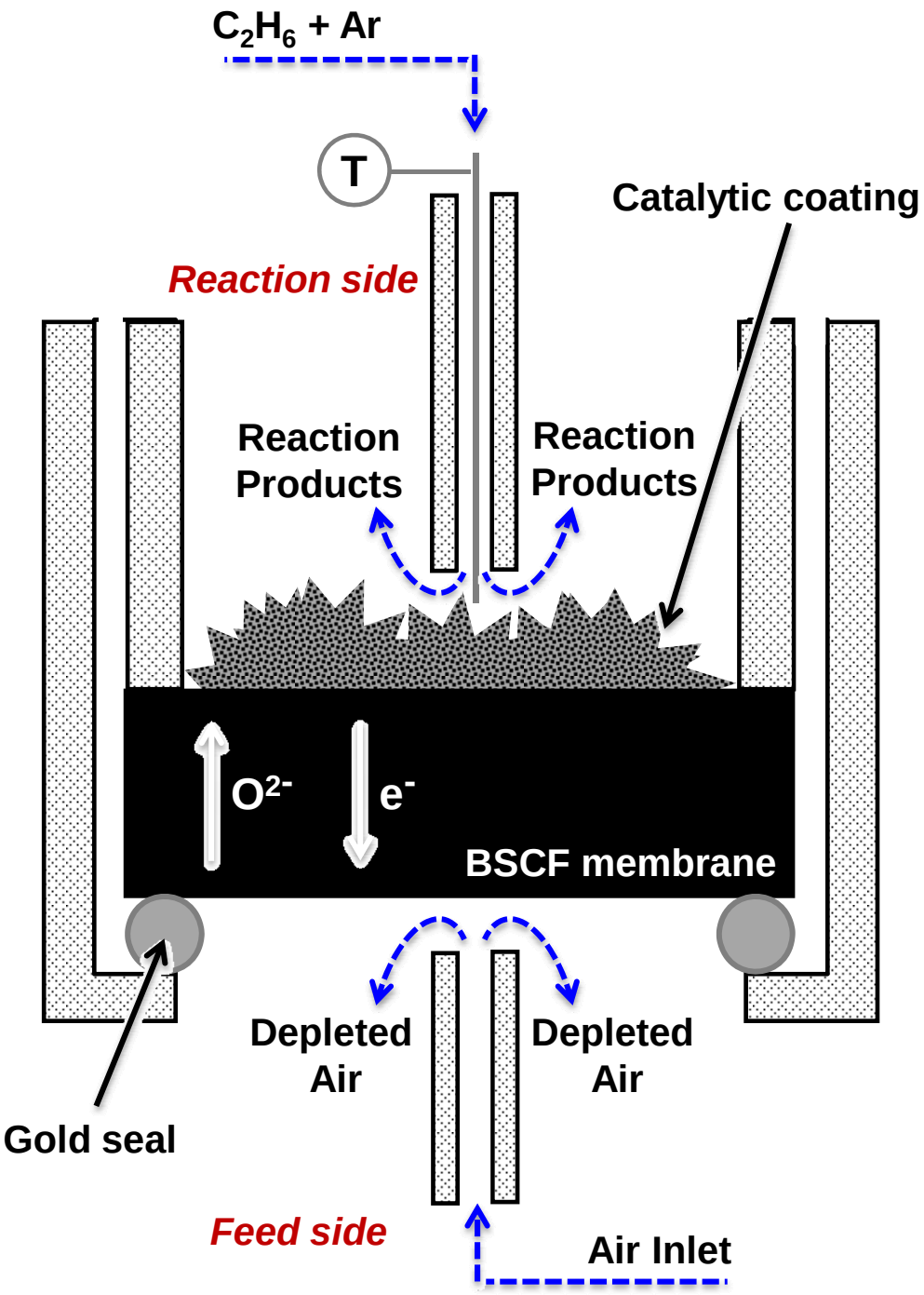
C_2H_6 + Ar
T
Catalytic coating
Reaction side
Reaction Products
Reaction Products
O^{2-}
e^-
BSCF membrane
Depleted Air
Depleted Air
Gold seal
Feed side
Air Inlet

Figure 3

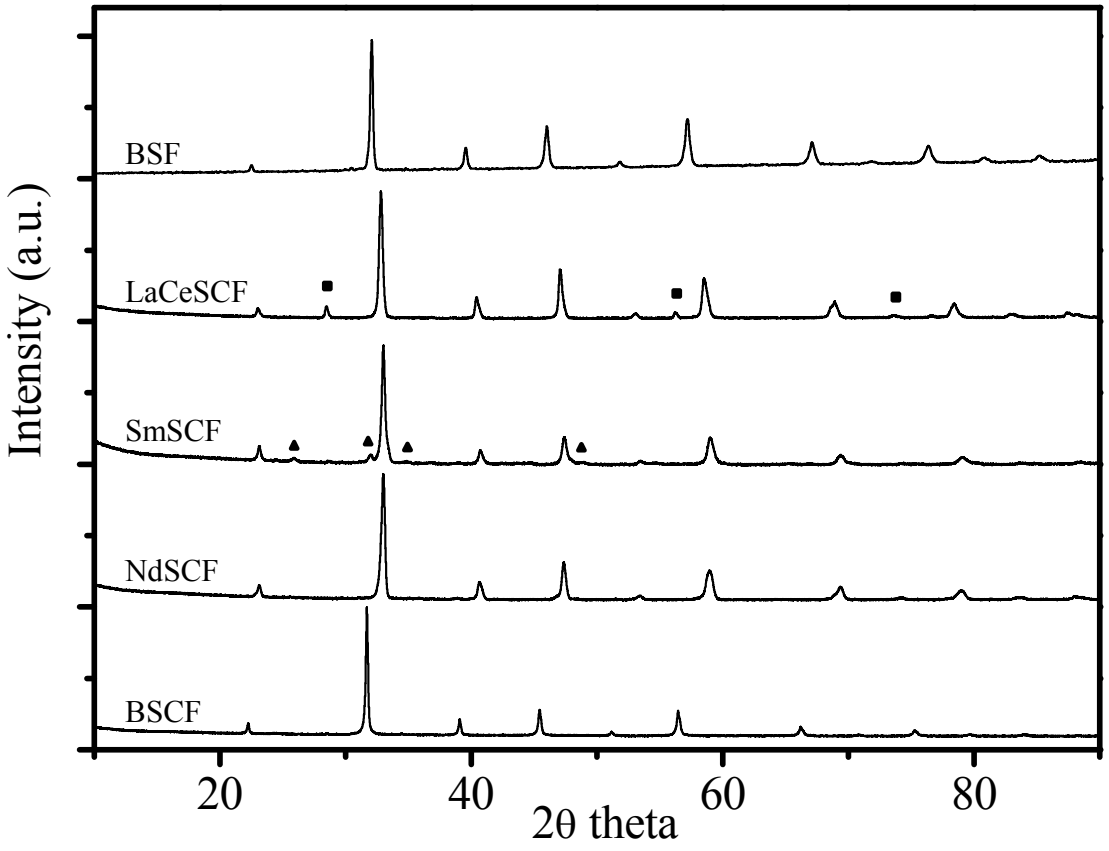
BSF
LaCeSCF
SmSCF
NdSCF
BSCF
Intensity (a.u.)
20
40
60
80
2θ theta

Figure 4

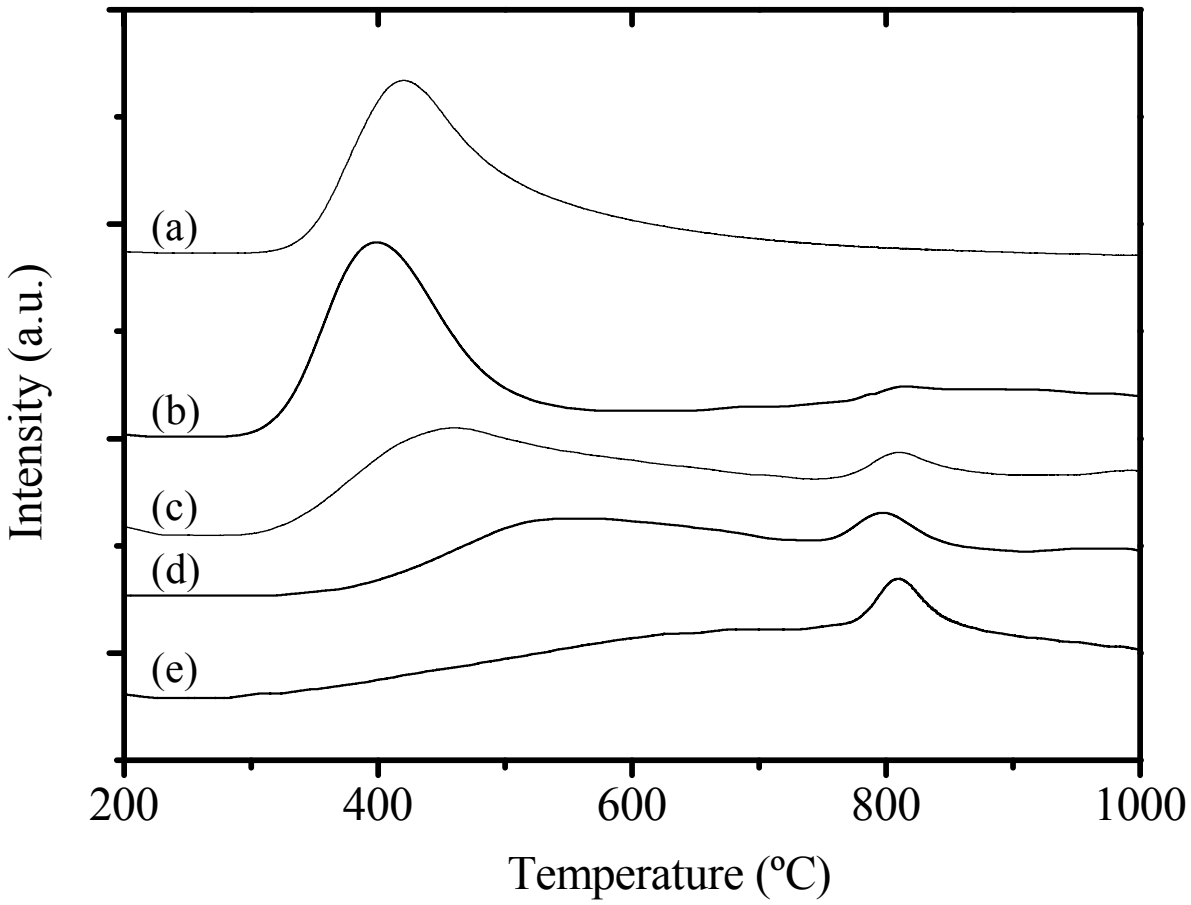

Figure 5

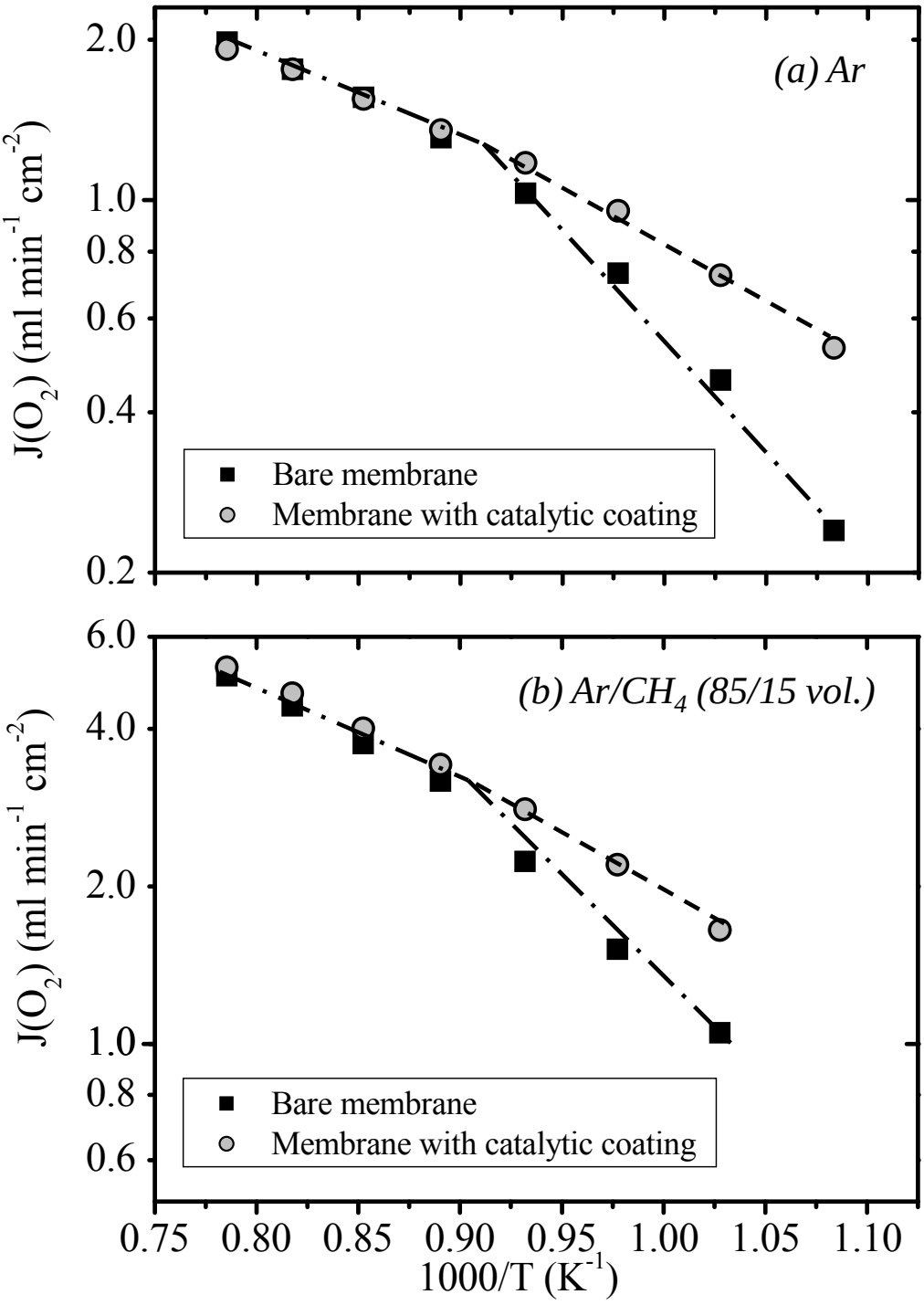
(a) Ar
J(O2) (ml min-1 cm-2)
2.0
1.0
0.8
0.6
0.4
0.2
Bare membrane
Membrane with catalytic coating
(b) Ar/CH4 (85/15 vol.)
J(O2) (ml min-1 cm-2)
6.0
4.0
2.0
1.0
0.8
0.6
Bare membrane
Membrane with catalytic coating
0.75 0.80 0.85 0.90 0.95 1.00 1.05 1.10
1000/T (K-1)

Figure 6

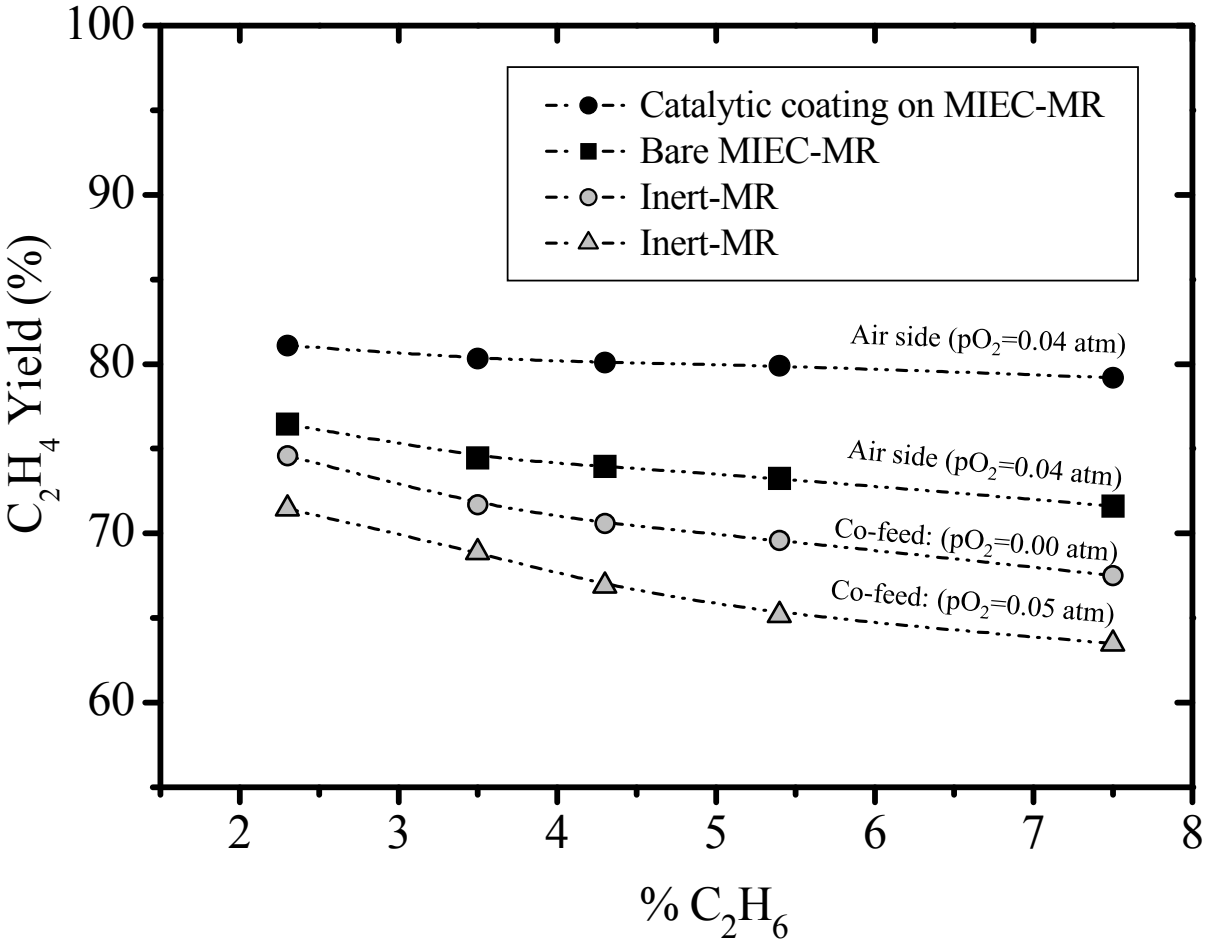
100
90
80
70
60
2
3
4
5
6
7
8
C_2H_4 Yield (%)
% C_2H_6
Catalytic coating on MIEC-MR
Bare MIEC-MR
Inert-MR
Inert-MR
Air side (pO_2=0.04 atm)
Air side (pO_2=0.04 atm)
Co-feed: (pO_2=0.00 atm)
Co-feed: (pO_2=0.05 atm)

Figure 7

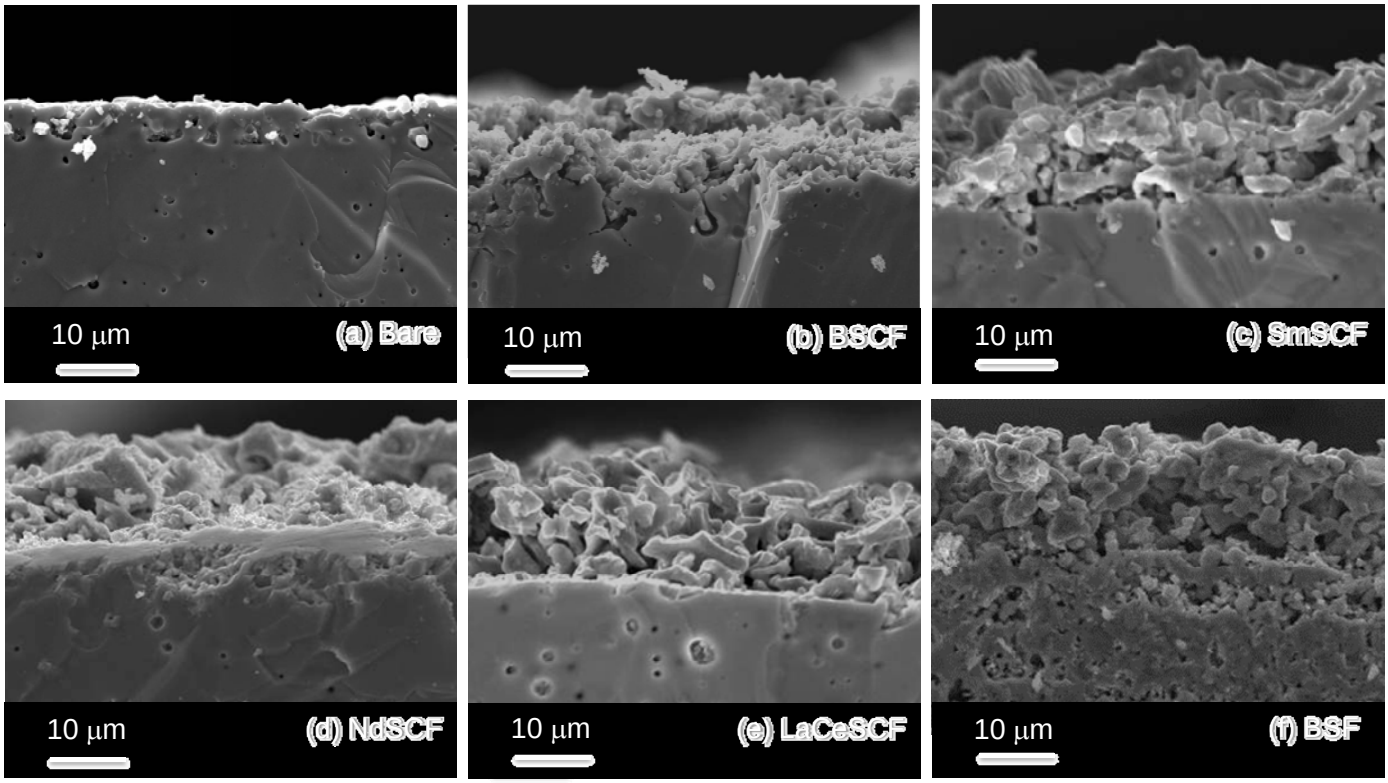
10 μm
(a) Bare
10 μm
(b) BSCF
10 μm
(c) SmSCF
10 μm
(d) NdSCF
10 μm
(e) LaCeSCF
10 μm
(f) BSF

Figure 8

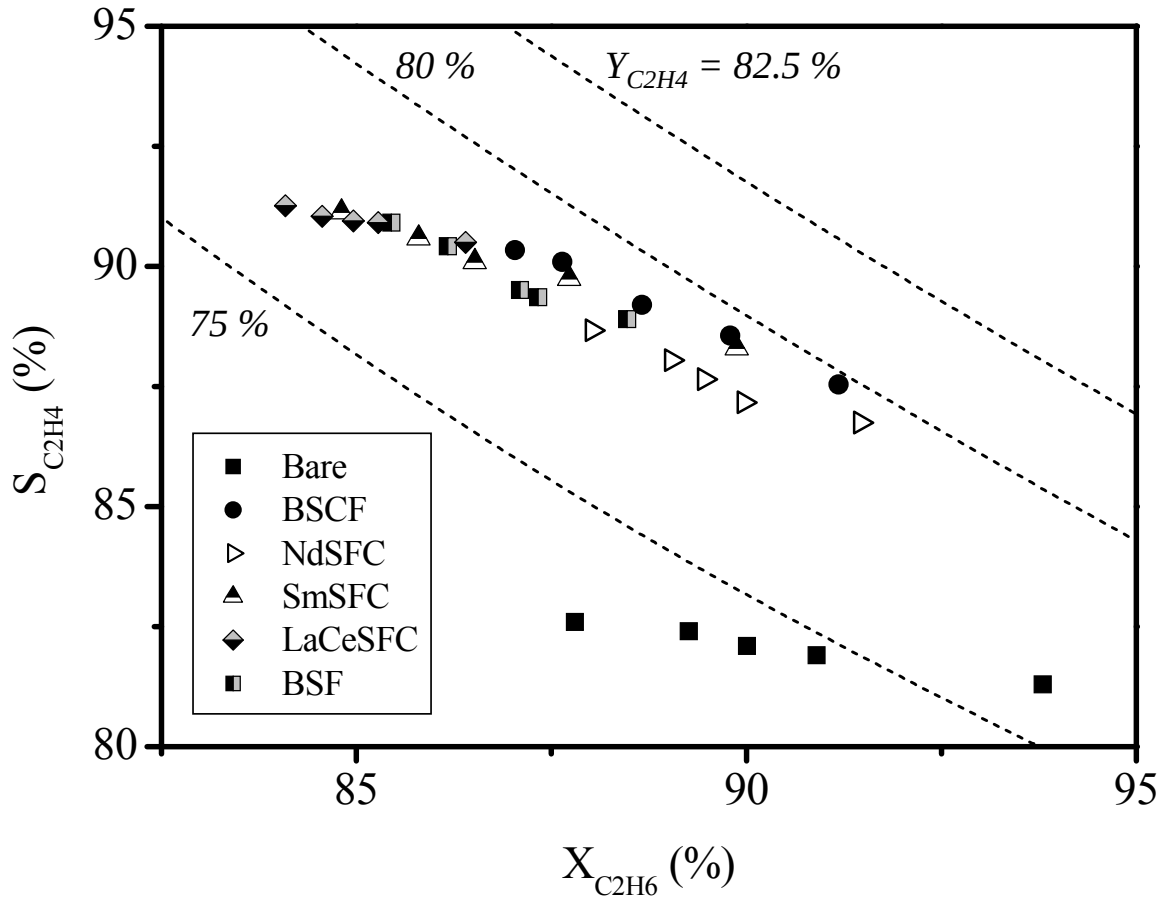
95
90
85
80
85
90
95
80 %
Y_{C2H4} = 82.5 %
75 %
Bare
BSCF
NdSFC
SmSFC
LaCeSFC
BSF
S_{C2H4} (%)
X_{C2H6} (%)

Figure 9

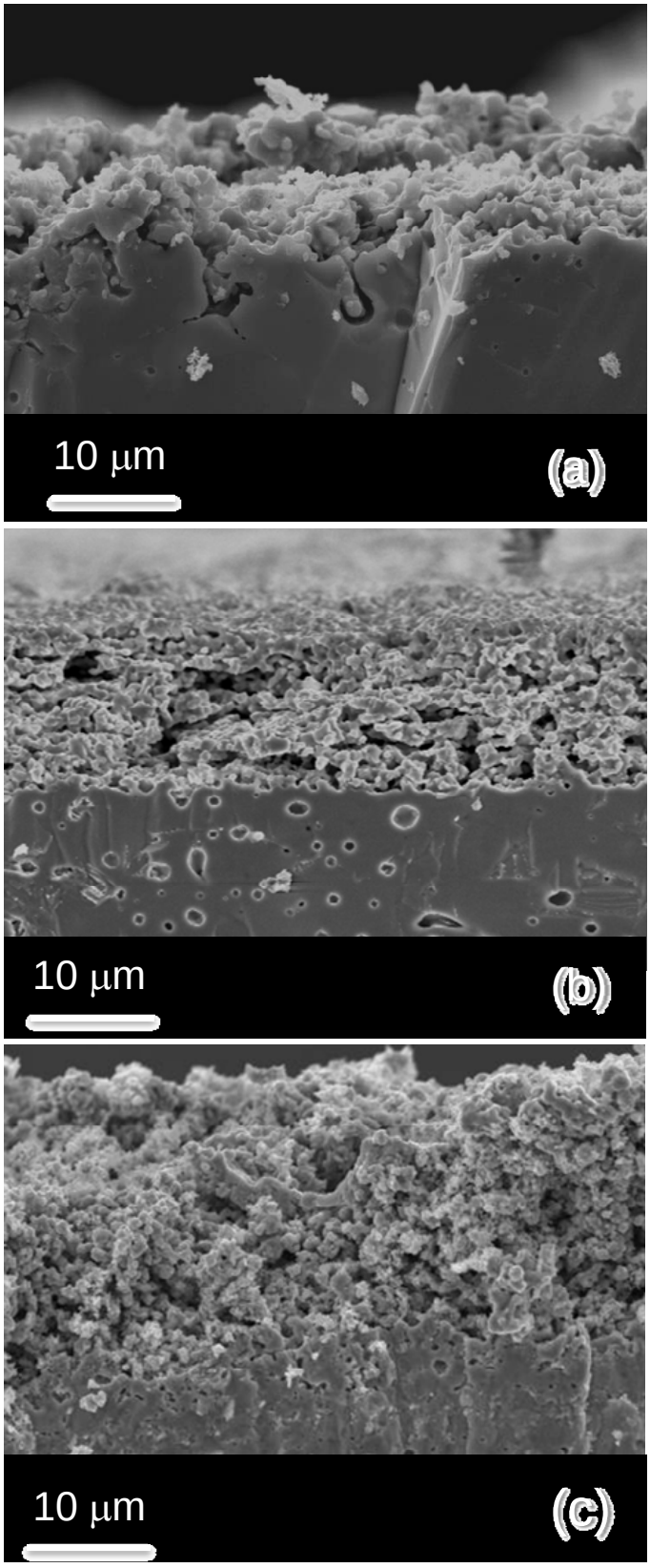

Figure 10

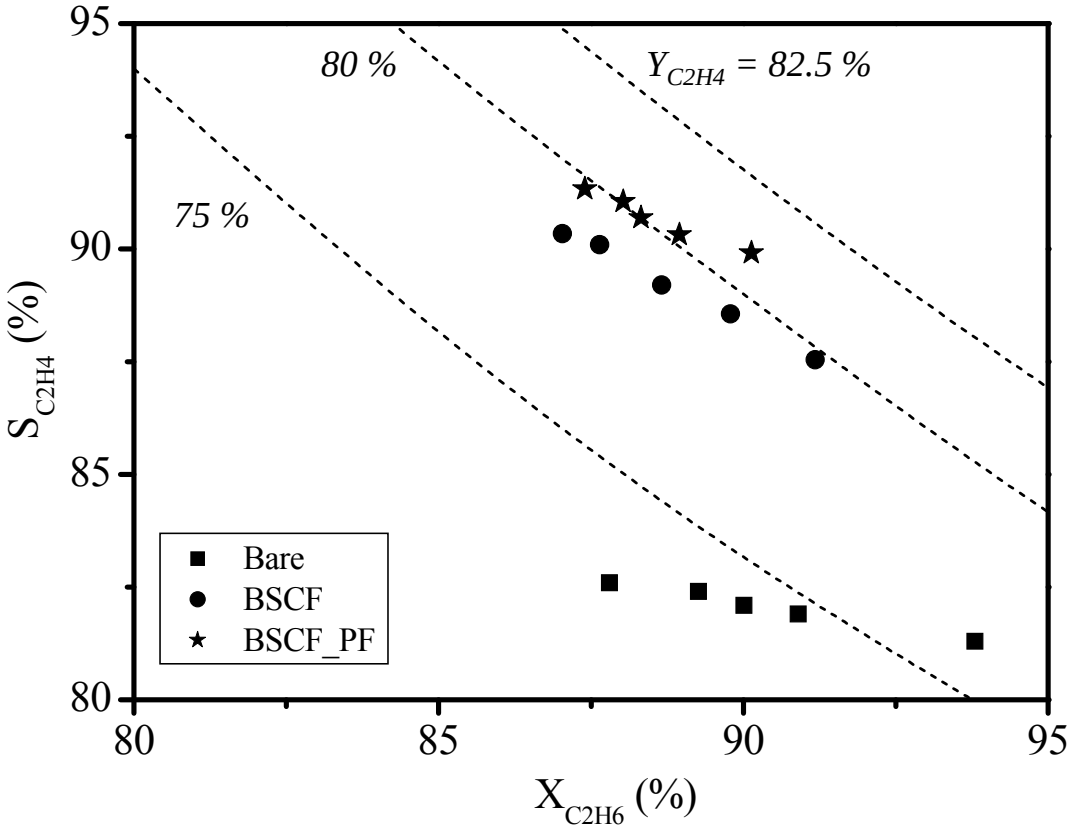
95
90
85
80
80
85
90
95
80 %
75 %
Y_{C2H4} = 82.5 %
Bare
BSCF
BSCF_PF
S_{C2H4} (%)
X_{C2H6} (%)

Figure 11

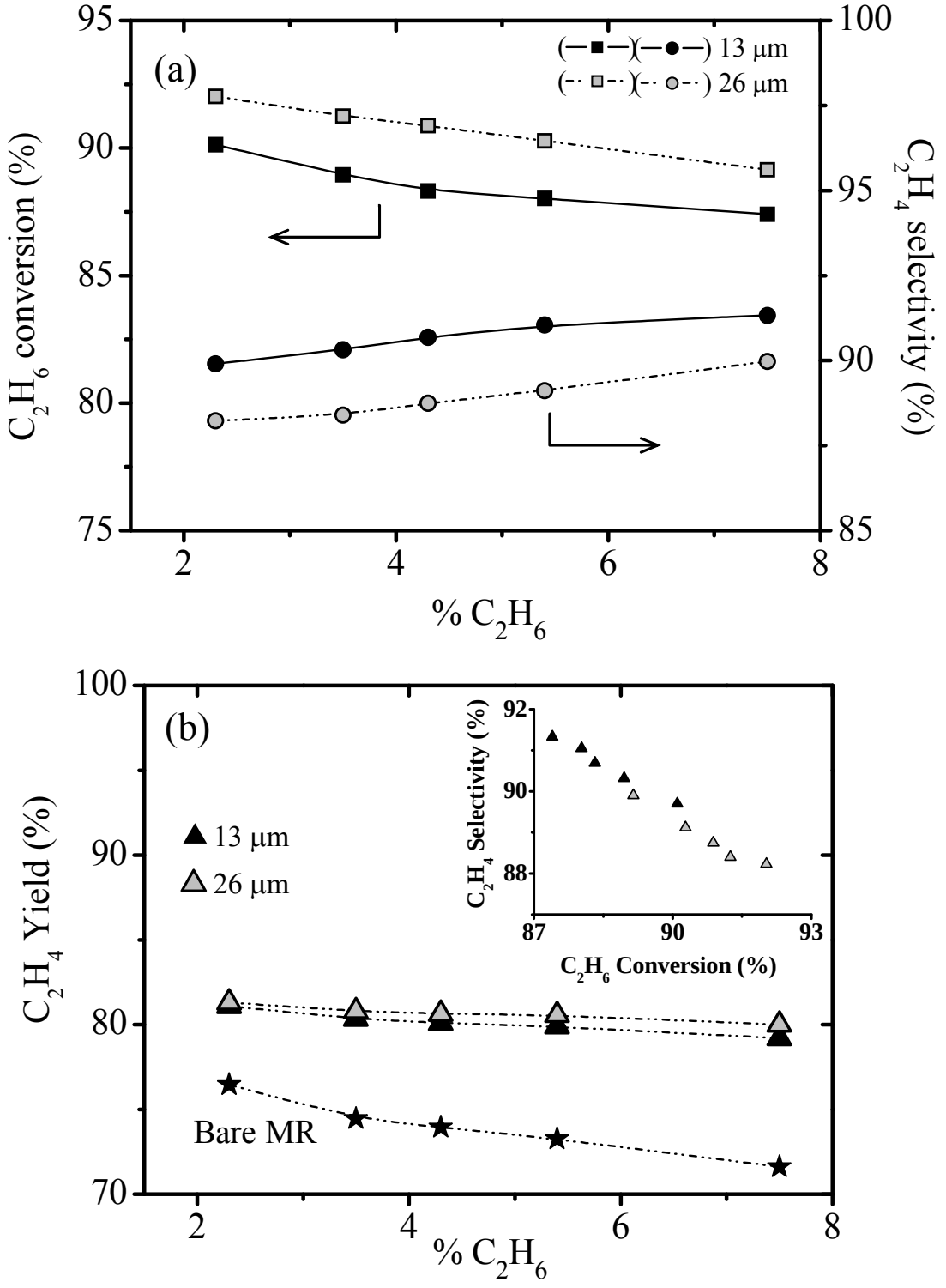
(a)
(—■—)(—●—) 13 μm
(-·□·-)(-·○·-) 26 μm
C_2H_6 conversion (%)
C_2H_4 selectivity (%)
% C_2H_6
(b)
13 μm
26 μm
Bare MR
C_2H_4 Yield (%)
C_2H_4 Selectivity (%)
C_2H_6 Conversion (%)
% C_2H_6

Figure 12

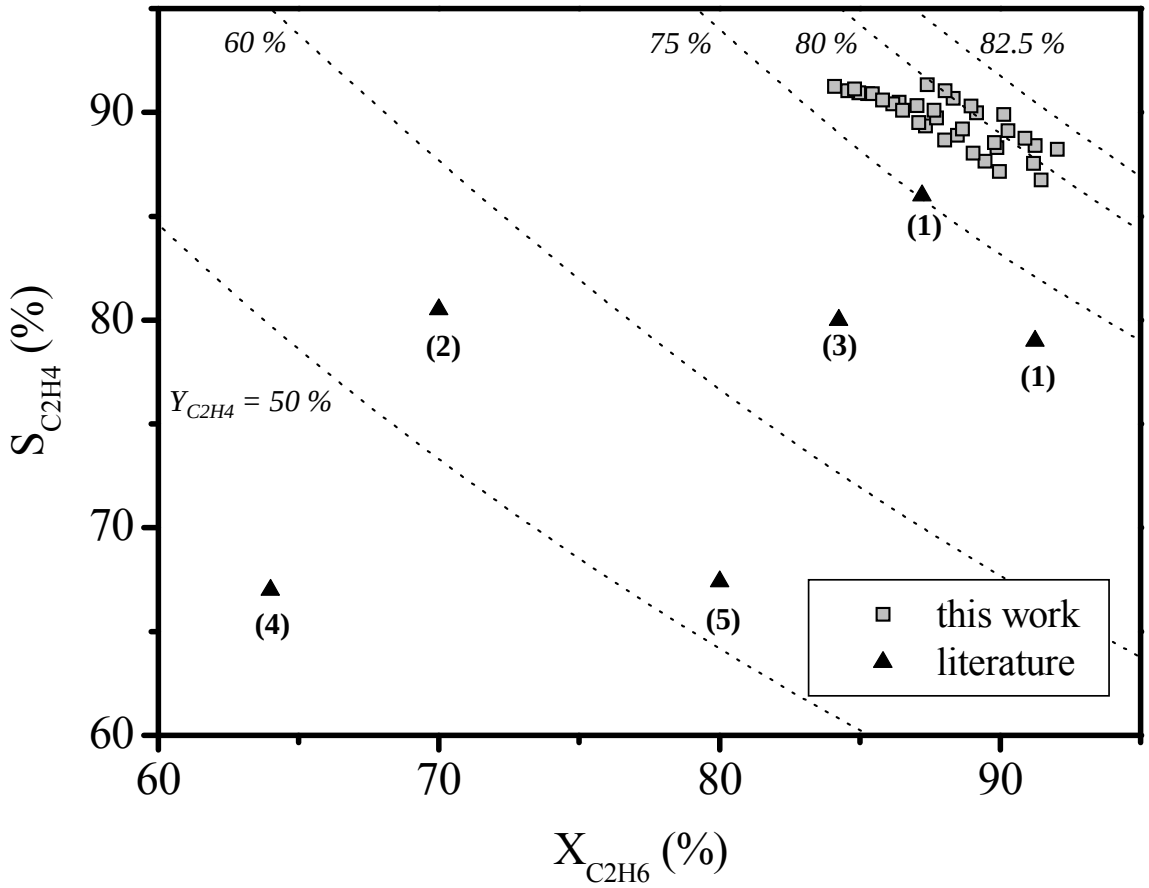
60 %
75 %
80 %
82.5 %
90
80
70
60
S_{C2H4} (%)
Y_{C2H4} = 50 %
(1)
(2)
(3)
(1)
(4)
(5)
this work
literature
60
70
80
90
X_{C2H6} (%)

Figure 13

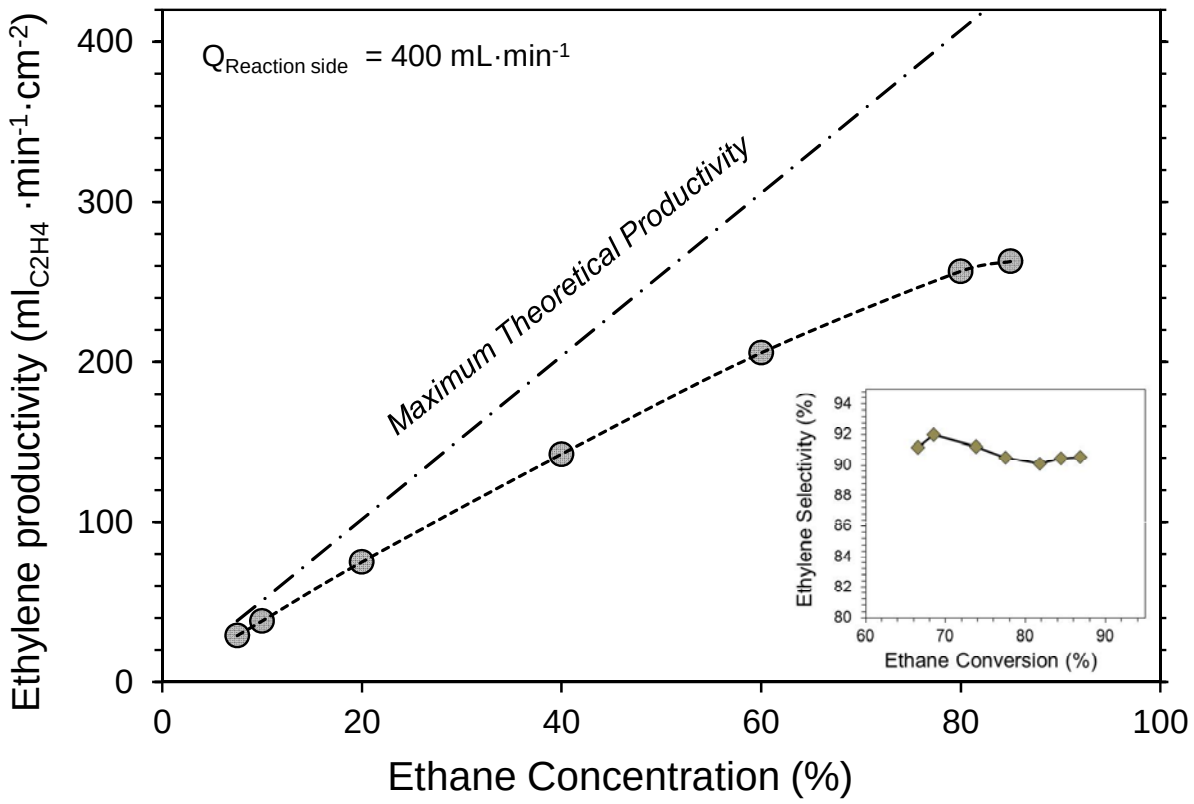
Q Reaction side = 400 mL·min-1
Maximum Theoretical Productivity
Ethylene productivity (mlC2H4 ·min-1·cm-2)
Ethane Concentration (%)
Ethylene Selectivity (%)
Ethane Conversion (%)

Tables

Table 1. Estimation of the activation energy $(E_a)^*$ (kJ mol^{-1}) regard to oxygen permeation flux. Different catalytic BSCF membrane reactors.

Sweep gas	***Membrane reactor***	***High T***	***Low T***
Ar	Bare (polished surface)	32.4 ± 1.2	79.9 ± 3.5
	BSCF_PF catalytic layer (~13 μm)	27.0 ± 1.0	45.2 ± 2.2
Ar/CH_4 (85/15 vol.)	Bare (polished surface)	36.1 ± 3.2	65.4 ± 2.6
	BSCF_PF catalytic layer (~13 μm)	34.3 ± 1.4	44.6 ± 1.6

Table 2. Catalytic performance of the different BSCF membrane reactors. T=850 ºC, ethane diluted with argon (C_2H_6 = 7.5 %)

Catalytic Layer				***ODHE Performance***								
Label	*Thickness (μm)[(a)]*	*Composition*	*$T_{Calcination}$ (ºC)*	*Y_{C2H4} (%)*	*X_{C2H6} (%)*	*Selectivity (%)*				*H_2*	*C_2H_4 productivity*	*C- balance*
						C_2H_4	***C_2H_6***	*CH_4*	*C_4*	*[% v/v]*	*(ml/min cm^2)*	*(%)*
Bare	---	---	----	73.1	87.8	83.3	3.7	3.4	9.3	11.8	28.7	± 3.7
LaCeSCF	13	$La_{0.5}Ce_{0.1}Sr_{0.4}Co_{0.8}Fe_{0.2}O_{3-\delta}$	1050	78.1	85.6	91.2	1.6	1.2	5.8	12.4	30.1	± 2.5
SmSCF	11	$Sm_{0.6}Sr_{0.4}Co_{0.8}Fe_{0.2}O_{3-\delta}$	1050	77.3	84.9	91.1	1.8	0.6	6.3	12.8	30.3	± 1.2
NdSCF	12	$Nd_{0.6}Sr_{0.4}Co_{0.8}Fe_{0.2}O_{3-\delta}$	1050	76.7	86.5	88.7	1.6	2.2	7.0	12.1	30.6	± 2.3
BSF	14	$Ba_{0.6}Sr_{0.4}FeO_{3-\delta}$	1050	77.7	85.7	90.7	1.4	0.9	6.8	12.3	30.5	± 1.2
BSCF	12	$Ba_{0.5}Sr_{0.5}Co_{0.8}Fe_{0.2}O_{3-\delta}$	1010	79.6	88.2	90.3	1.8	1.3	6.3	11.3	30.8	± 1.1
BSCF-PF[(b)]	13	$Ba_{0.5}Sr_{0.5}Co_{0.8}Fe_{0.2}O_{3-\delta}$	1010	79.9	87.5	91.3	1.8	1.4	5.3	11.6	31.3	± 1.0
BSCF-PF[(b)]	26	$Ba_{0.5}Sr_{0.5}Co_{0.8}Fe_{0.2}O_{3-\delta}$	1010	80.3	89.2	90.0	1.9	1.9	5.6	10.9	31.5	± 1.1

(a) Standard deviation, σ ± 3 %.
(b) Catalytic layer with higher porosity achieved to the incorporation in the screen-printing ink of pore former.

References

[1] M. M. Bhasin *Topics in Catalysis*. **2003**, 23, 145-149.
[2] H. Zimmermann, R. Walzl in *Ethylene, Vol.*, Wiley-VCH Verlag GmbH & Co. KGaA, **2000**.
[3] M. M. Bhasin, J. H. McCain, B. V. Vora, T. Imai, P. R. Pujadó *Applied Catalysis A: General*. **2001**, 221, 397-419.
[4] T. Blasco, J. M. L. Nieto *Applied Catalysis A:General*. **1997**, 157, 117-142.
[5] F. Cavani, N. Ballarini, A. Cericola *Catalysis Today*. **2007**, 127, 113-131.
[6] R. K. Grasselli *Catalysis Today*. **1999**, 49, 141-153.
[7] W. Yang, H. Wang, X. Zhu, L. Lin *Topics in Catalysis*. **2005**, 35, 155-167.
[8] F. T. Akin, Y. S. Lin *Journal of Membrane Science*. **2002**, 209, 457-467.
[9] H. J. M. Bouwmeester *Catalysis Today*. **2003**, 82, 141-150.
[10] C. M. Chen, D. L. Bennett, M. F. Carolan, E. P. Foster, W. L. Schinski, D. M. Taylor in *ITM Syngas ceramic membrane technology for synthesis gas production, Vol. Volume 147* (Eds.: B. Xinhe, X. Yide), Elsevier, **2004**, pp.55-60.
[11] J. A. Dalmon, A. Cruz-López, D. Farrusseng, N. Guilhaume, E. Iojoiu, J. C. Jalibert, S. Miachon, C. Mirodatos, A. Pantazidis, M. Rebeilleau-Dassonneville, Y. Schuurman, A. C. van Veen *Applied Catalysis A: General*. **2007**, 325, 198-204.
[12] M. P. Lobera, S. Escolástico, J. M. Serra *ChemCatChem*. **2011**, 3, 1503-1508.
[13] A. Machocki, A. Denis *Chemical Engineering Journal*. **2002**, 90, 165-172.
[14] M. Rebeilleau-Dassonneville, S. Rosini, A. C. van Veen, D. Farrusseng, C. Mirodatos *Catalysis Today*. **2005**, 104, 131-137.
[15] Z. Shao, H. Dong, G. Xiong, Y. Cong, W. Yang *Journal of Membrane Science*. **2001**, 183, 181-192.
[16] H. H. Wang, Y. Cong, W. S. Yang *Catalysis Letters*. **2002**, 84, 101-106.
[17] H. H. Wang, C. Tablet, T. Schiestel, J. Caro *Catalysis Today*. **2006**, 118, 98-103.
[18] J. Sunarso, S. Baumann, J. M. Serra, W. A. Meulenberg, S. Liu, Y. S. Lin, J. C. D. da Costa *Journal of Membrane Science*. **2008**, 320, 13-41.
[19] J. Vente, S. McIntosh, W. Haije, H. Bouwmeester *Journal of Solid State Electrochemistry*. **2006**, 10, 581-588.
[20] S. Baumann, J. M. Serra, M. P. Lobera, S. Escolástico, F. Schulze-Küppers, W. A. Meulenberg *Journal of Membrane Science*. **2011**, 377, 198-205.
[21] A. Leo, S. Smart, S. Liu, J. C. Diniz da Costa *Journal of Membrane Science*. **2011**, 368, 64-68.
[22] O. Büchler, J. M. Serra, W. A. Meulenberg, D. Sebold, H. P. Buchkremer *Solid State Ionics*. **2007**, 178, 91-99.
[23] Z. Shao, W. Yang, Y. Cong, H. Dong, J. Tong, G. Xiong *Journal of Membrane Science*. **2000**, 172, 177-188.
[24] S. Escolástico, V. B. Vert, J. M. Serra *Chemistry of Materials*. **2009**, 21, 3079-3089.
[25] J. M. Serra, V. B. Vert, M. Betz, V. A. C. Haanappel, W. A. Meulenberg, F. Tietz *Journal of The Electrochemical Society*. **2008**, 155, B207-B214.
[26] J. M. Serra, V. B. Vert *Chemsuschem*. **2009**, 2, 957-961.
[27] V. B. Vert, J. M. Serra *Fuel Cells*. **2009**, 9, 663-678.
[28] D. N. Mueller, R. A. De Souza, J. Brendt, D. Samuelis, M. Martin *Journal of Materials Chemistry*. **2009**, 19, 1960-1963.
[29] X. Yang, L. Luo, H. Zhong *Catalysis Communications*. **2005**, 6, 13-17.
[30] W. Zhou, R. Ran, Z. Shao, W. Zhuang, J. Jia, H. Gu, W. Jin, N. Xu *Acta Materialia*. **2008**, 56, 2687-2698.

[31] S. Haag, A. C. van Veen, C. Mirodatos *Catalysis Today*. **2007**, 127, 157-164.
[32] J. M. Gozálvez-Zafrilla, A. Santafé-Moros, S. Escolástico, J. M. Serra *Journal of Membrane Science*. **2011**, 378, 290-300.
[33] M. P. Lobera, S. Valero, J. M. Serra, S. Escolástico, E. Argente, V. Botti *Chemical Engineering Science*. **2011**, 66, 6308-6312.
[34] I. García-Torregrosa, M. P. Lobera, C. Solís, P. Atienzar, J. M. Serra *Advanced Energy Materials*. **2011**, 1, 618-625.
[35] M. P. Lobera, J. M. Serra, S. P. Foghmoes, M. Søgaard, A. Kaiser *Journal of Membrane Science*.
[36] M. a. Balaguer, C. Solís, J. M. Serra *Chemistry of Materials*. **2011**, 23, 2333-2343.
[37] E. M. Kennedy, N. W. Cant *Applied Catalysis*. **1991**, 75, 321-330.
[38] O. Czuprat, S. Werth, S. Schirrmeister, T. Schiestel, J. Caro *ChemCatChem*. **2009**, 1, 401-405.
[39] J. Yi, M. Schroeder *Journal of Membrane Science*. **2011**, 378, 163-170.

GRAPHICAL ABSTRACT